THE JOURNAL OF PHYSICAL CHEMISTRY A

Article

Cite This: J. Phys. Chem. A 2019, 123, 4406−4418

pubs.acs.org/JPCA

Configuration Space Analysis of the Specific Rotation of Helicenes

Tal Aharon and Marco Caricato*

Department of Chemistry, University of Kansas, 1567 Irving Hill Road, Lawrence, Kansas 66045, United States

Supporting Information

ABSTRACT: In this work, we present an analysis of a series of helicene molecules to determine the driving forces for their large specific rotation, $[\alpha]_\omega$, and probe the effects of functionalization. The analysis is done in the configuration space of the molecular orbitals (MOs), and it allows us to decompose $[\alpha]_\omega$ into the component transition electric and magnetic dipoles from single MO excitations. We find that $[\alpha]_\omega$ for helicene molecules may be described by three sets of transitions based on the orientation of the magnetic dipole with respect to the helical axis: parallel, orthogonal, or tilted. The transitions with the magnetic dipole parallel to the helical axis, corresponding to a delocalized motion of the electron along the body of the helix, provide the largest contributions and determine the sign and magnitude of $[\alpha]_\omega$. Functionalization has a complex effect on $[\alpha]_\omega$, which is dependent on the number of substituent groups and their electron directing strength. Furthermore, we test the $[\alpha]_\omega$ decomposition analysis using localized MOs (Boys and Pipek−Mezey). We show that localization schemes may be useful to simplify the interpretation of the $[\alpha]_\omega$ decomposition, but they are best used when the electronic transitions involve relatively small chromophoric groups.

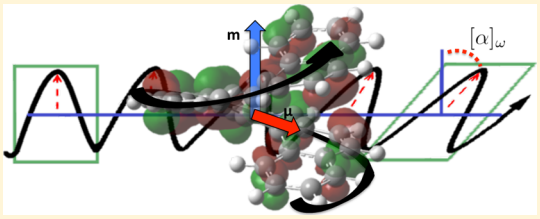

1. INTRODUCTION

The study of optically active molecules is of continuous interest because of the fundamental role chiral molecules play in living organisms, as building blocks of life (i.e., L-amino acids and D-sugars) as well as drugs.[1] Given the homochiral nature of biological compounds, the correct determination of the absolute configuration is paramount, for instance, for the synthesis of natural products with favorable biological activity. Chiroptical spectroscopy and theoretical simulations have been very successful at this task, and they have become an essential tool in the pharmaceutical industry. This work focuses on the oldest of these measurements, that of the specific rotation $[\alpha]_\omega$, whose sign is directly related to the absolute configuration of a particular enantiomer. The accurate calculation of $[\alpha]_\omega$ is difficult as this property is very sensitive to the molecular structure and the interaction with the environment. Nevertheless, great progress has been made over the past two decades, including the use of modern density functional theory (DFT) and coupled cluster methods.[2−17]

Despite this progress, a chemically intuitive understanding of the relationship between the absolute configuration of a chiral molecule and the $[\alpha]_\omega$ sign and magnitude is still lacking. Various groups have developed models to determine structure−property relationships. For instance, Autschbach and co-workers performed a decomposition of $[\alpha]_\omega$ via localized orbital contributions to the diagonal elements of the Rosenfeld tensor. This work showed that the large $[\alpha]_\omega$ of (1*S*,4*S*)-norbornenone is due to electron delocalization between the C═O and C═C chromophores.[18] Kahr and co-workers extended the analysis of optical activity to include nonchiral molecules through a simple and effective Hückel theory decomposition.[19,20] Wiberg examined the effect on $[\alpha]_\omega$ of the rotation of the torsional angle of terminally substituted 1,4-pentadiene (C═C to C═X interactions, where X = C, O, NH, and S) and found a dependence on the electronegativity of X.[21,22] We have also introduced a method of decomposing $[\alpha]_\omega$ in terms of transition electric and magnetic dipole contributions, called the $\tilde{S}_k$ method (discussed in Section 2).[23,24] We showed that a limited number of orbital transitions can be used to describe $[\alpha]_\omega$ for molecules with strong chromophoric groups[23] and that changes in $[\alpha]_\omega$ due to conformational flexibility are dominated by a small number of transitions,[24] thus simplifying the interpretation of the structure−property relationship.

In this work, we apply the $\tilde{S}_k$ analysis to a series of standard and functionalized helicenes of various lengths. These molecules are composed of a series of fused phenyl rings and have been studied extensively both computationally and experimentally.[25] They are known for their intense chiroptical response,[26] nonlinear optical activity,[27,28] and self-assembly.[25] They have also garnered interest as redox-active chiral switches[29,30] and have been functionalized extensively to modulate their optical properties.[31] The Avarvari group created many helicene derivatives to investigate the effect of functionalization on its electronic properties.[31] Crassous and co-workers successfully synthesized novel organometallic helicenes[31−35] and showed that the electronic circular dichroism (ECD) spectrum reversibly switches under redox stimuli.[29,30] Autschbach and co-workers performed theoretical simulations of ECD and UV/vis absorption spectra of these organometallic helicenes to elucidate the role of charge-transfer excitations in the redox switching mechanism.[36−40]

Received: February 25, 2019
Revised: April 20, 2019
Published: May 1, 2019

DOI: 10.1021/acs.jpca.9b01823
J. Phys. Chem. A 2019, 123, 4406−4418

Nakai, Mori, and Inoue also studied the ECD spectra of helicenes and analyzed the rotatory strength of various absorption bands based on the relative orientation of the transition electric and magnetic dipole moments.[41−43] In this work, we extend these analyses to the specific rotation of standard and functionalized helicenes through the $\tilde{S}_k$ method. We aim to understand how $[\alpha]_\omega$ changes with length and pitch of the helical backbone, and with the introduction of electron-withdrawing or electron-donating groups, which may lead to guidelines for the development of compounds with desired electronic responses. The $\tilde{S}_k$ analysis reveals that the $[\alpha]_\omega$ magnitude is driven by the delocalized motion of the electron along the entire backbone of the helicene, resulting in strong magnetic dipole contributions. Functionalization directs the orbital density toward or away from the substituent groups, affecting $[\alpha]_\omega$ based on the electron push/pull strength and on the degree of orbital overlap between the groups.

Because $[\alpha]_\omega$ is invariant to unitary transformations within the occupied and virtual molecular orbital (MO) subspaces, we also explore the use of localized MOs (LMOs) [with the Boys[44,45] and Pipek−Mezey[46] (PM) approaches] for the $\tilde{S}_k$ decomposition of the specific rotation. We find that LMOs may provide a more chemically intuitive picture than canonical MOs (CMOs); however, they are best employed when the molecule possesses small, localized chromophores.

This work is organized as follows: Section 2 reviews the $\tilde{S}_k$ method and the derivation of LMOs, Section 3 describes the computational protocol, Section 4 presents the results of the calculations, and Section 5 contains a discussion of these results and concluding remarks.

2. THEORY

From Rosenfeld's derivation, the specific rotation $[\alpha]_\omega$ can be expressed using a sum-over-states (SOS) formula as

$$[\alpha]_\omega = -\frac{C_\omega}{M}\sum_{n=1}^{N_{ex}}\left(\frac{R_n}{\omega_n - \omega} + \frac{R_n^*}{\omega_n + \omega}\right) \tag{1}$$

where N_{ex} is the number of excited states, ω_n is the transition energy to the nth excited state, ω is the frequency of the incident light, M is the molecular mass, and C_ω is a proportionality constant to obtain the common units of deg [dm (g/mL)]$^{-1}$.[47] The rotatory strength R_n is related to the differential absorption of left and right circularly polarized light measured in circular dichroism spectroscopy

$$R_n = \mathrm{Im}\left\{\sum_{i=1}^{3}\langle 0|\mu_i|\Psi_n\rangle\langle\Psi_n|m_i|0\rangle\right\} \tag{2}$$

where μ_i and m_i are the ith component of the electric and magnetic dipole operators, respectively, and Ψ_n is the nth excited state. Note that R_n is the dot product of the two transition dipoles. If the energy denominator was to be included into the definition of R_n, eq 1 may be written in a more compact form

$$[\alpha]_\omega = -\frac{C_\omega}{M}\sum_{n=1}^{N_{ex}}(\tilde{R}_n + \tilde{R}_n^*) \tag{3}$$

Equations 1−3 apply only in nonresonant conditions (i.e., ω far from ω_n), as is the case in this work.

The SOS equations are of little practical use because of the large number of excited states needed to converge the series in eq 3.[48] A more computationally efficient approach to calculate $[\alpha]_\omega$ is based on the linear response formalism.[12,17] In the case of single reference methods such as Hartree−Fock (HF) or Kohn−Sham DFT (KS DFT), $[\alpha]_\omega$ becomes

$$[\alpha]_\omega = -\frac{C_\omega}{M}\mathrm{Im}\left\{\sum_{i=1}^{3}\sum_{k=1}^{N_{ex}}(\langle 0|\mu_i|\phi_k\rangle\langle\phi_k|X_{m_i}^+|0\rangle + \text{c. c})\right\} \tag{4}$$

where k runs over singly excited Slater determinants ϕ_k. The $\langle\phi_k|X_{m_i}^+|0\rangle$ matrix element represents the electron density perturbed by the magnetic dipole, and it is evaluated by solving the coupled-perturbed (CP) HF or KS equations

$$\langle\phi_k|X_{m_i}^\pm|0\rangle = \sum_{l=1}^{N_{ex}}\langle\phi_k|(\hat{H} - E_0 \mp \omega)|\phi_l\rangle^{-1}\langle\phi_l|m_i|0\rangle \tag{5}$$

In order to interpret the specific rotation in terms of MO contributions, we may define a quantity similar to $\tilde{R}_n$ in the configuration space of the Slater determinants by switching the order of the sums in eq 4

$$\tilde{S}_k = \mathrm{Im}\left\{\sum_{i=1}^{3}\langle 0|\mu_i|\phi_k\rangle\langle\phi_k|X_{m_i}^+|0\rangle\right\} \tag{6}$$

so that eq 4 can be rewritten as a sum of $\tilde{S}_k$ rotatory strengths

$$[\alpha]_\omega = -\frac{C_\omega}{M}\sum_{k=1}^{N_{ex}}(\tilde{S}_k + \tilde{S}_k^*) \tag{7}$$

Because $\tilde{S}_k$ is also written as a dot product between two vectors, its magnitude and sign depend on the magnitude of the vectors and the angle θ between them. The advantage of the linear response formalism over the SOS formula is that the Slater determinant contributions to $[\alpha]_\omega$ (and thus the $\tilde{S}_k$ values) can be computed all at once by solving the linear system of equations in eq 5.

In Section 4, we proceed to analyze the origin of $[\alpha]_\omega$ of each molecule by the components of the $\tilde{S}_k$ dot product as well as the involved occupied and virtual MOs with eqs 6 and 7. One can focus on the largest $\tilde{S}_k$ contributions to the specific rotation to obtain a qualitative understanding of how individual orbital transitions affect this property, which may provide key insights on the structure−property relations in chiroptical spectroscopy. For clarity of discussion, in the rest of the paper, we refer to "$\tilde{S}_k$ contributions" to $[\alpha]_\omega$ even if the values reported are actually $\tilde{S}_k + \tilde{S}_k^*$ as in eq 7 and we use "magnetic dipole" contributions when discussing the $\langle\phi_k|X_{m_i}^+|0\rangle$ matrix elements in eq 6.

The Rosenfeld tensor and $[\alpha]_\omega$ are invariant under unitary transformations within the occupied MO and virtual MO subspaces, respectively. Therefore, it may be convenient to express $\tilde{S}_k$ using different choices of MO basis, beyond that of CMOs, as different bases may provide a smaller number of $\tilde{S}_k$ contributions to $[\alpha]_\omega$, or a more chemically intuitive picture. LMOs are often utilized for this purpose. Therefore, we consider two popular choices of LMOs: Boys[44,45] and PM.[46] The former are obtained by maximizing the distance between orbital centroids

$$\sum_{j=1}^{N_{MO}}\sum_{i>j}^{N_{MO}}[\langle i|\mathbf{r}|i\rangle - \langle j|\mathbf{r}|j\rangle]^2 \tag{8}$$

DOI: 10.1021/acs.jpca.9b01823
J. Phys. Chem. A 2019, 123, 4406−4418

where N_{MO} is the number of MOs in the subspace. The PM localization is based on the definition of a localization parameter d_i, which counts how many atoms are spanned by the ith MO

$$d_i = \left[\sum_{A=1}^{N_{at}} (Q_A^i)^2\right]^{-1} \tag{9}$$

where N_{at} is the number of atoms in the molecule and Q_A^i is the Mulliken population of orbital i on atom A. From d_i, one can define a mean delocalization of all MOs in the subspace

$$D = N_{MO}\left(\sum_{i=1}^{N_{MO}} d_i^{-1}\right)^{-1} \tag{10}$$

and the LMOs are obtained by minimization of D. Both localization techniques scale as $O(N^3)$, where N is the atomic basis set size, as they require the evaluation of electric dipole integrals. Thus, the computational cost of the MO localization is small compared to the solution of the self-consistent field (SCF) and CP equations.

3. COMPUTATIONAL DETAILS

All calculations were performed with a development version of the GAUSSIAN suite of programs.[49] Geometries were optimized using the CAM-B3LYP/aug-cc-pVDZ model chemistry with D3 dispersion corrections.[50,51] Calculations of specific rotation were performed at the sodium-D line (ω = 589.3 nm) with the B3LYP[52−54]/p-3-21G level of theory in the length gauge formalism using gauge-including atomic orbitals.[16,55,56] The p-3-21G basis set is built by augmenting the standard 3-21G basis set with p-type diffuse functions from the standard aug-cc-pVDZ basis set. This unorthodox choice is based on the previous work that showed how diffuse functions are the most important to obtain a good description of $[\alpha]_D$.[57] In the context of this study, using a reduced basis set is critical as this allows to reduce the number of $\tilde{S}_k$ contributions and to simplify the qualitative decomposition and analysis of $[\alpha]_D$ in terms of orbital transitions. Nevertheless, all $[\alpha]_D$ values computed with p-3-21G are in reasonable agreement with those obtained with the full aug-cc-pVDZ basis set (with errors on the order of 9−18%), thus justifying the use of this smaller set.

4. RESULTS

4.1. Localized Orbitals. As discussed in Section 2, the Rosenfeld tensor (and thus $[\alpha]_\omega$) can be decomposed in different MO bases, related by unitary transformations within the occupied MO or the virtual MO subspaces. Thus, we consider transformations of both the occupied and virtual MO subspaces, as well as transformation of only the occupied MO subspace, as this may be enough for the qualitative interpretation of the $[\alpha]_D$ tensor with the $\tilde{S}_k$ analysis. In summary, we obtain the $[\alpha]_\omega$ tensor and the corresponding $\tilde{S}_k$ values for five choices of MO basis: CMOs, Boys-localized occupied MOs (BO-LMOs), Boys-localized occupied and virtual MOs (BOV-LMOs), PM-localized occupied MOs (PMO-LMOs), and PM-localized occupied and virtual MOs (PMOV-LMOs). Given that the computational cost of the MO localization and of the tensor transformation is virtually negligible compared to the solution of the SCF and linear response equations, we evaluate $[\alpha]_D$ and $\tilde{S}_k$ with all five MO options for every calculation and choose the most appropriate for a specific system on-the-fly.

The first test case is (1*S*,4*S*)-norbornenone because this molecule has a very large $[\alpha]_D$, and previous studies have shown that it is dominated by a small number of electronic transitions.[18,23,58] In Figure 1, we report the cumulative contribution of the $\tilde{S}_k$ transitions to the total $[\alpha]_D$, separated according to their magnitude.

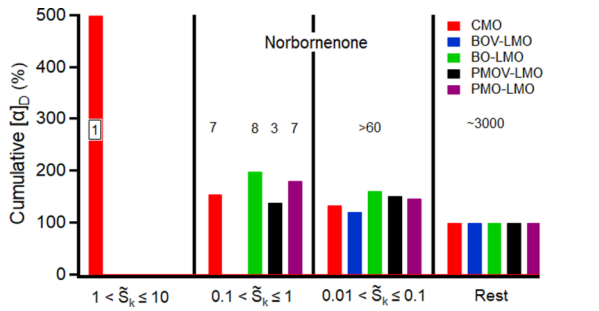

Figure 1. Plot of the cumulative % $\tilde{S}_k$ contributions to the total $[\alpha]_D$ for (1*S*,4*S*)-norbornenone with various choices of MO basis. The $\tilde{S}_k$ contributions are divided according to their magnitude as reported in the x axis labels, whereas the y axis reports the cumulative percent of $[\alpha]_D$ recovered by summing all $\tilde{S}_k$ in the current and larger-value ranges. The numbers on the bars indicate how many transitions fall within each range.

The CMO basis provides the most compact representation of $[\alpha]_D$, in the sense that a single transition is dominant, and it determines the sign. More transitions are necessary to reach the converged value of the rotation (e.g., 8 transitions are necessary to be within 50% of the converged value, and about 60 transitions to be within the 10% margin), but a single transition is enough for a qualitative discussion. The isodensity plots and corresponding vector representation of the electric and magnetic dipoles for this transition are reported in Figure S1 of the Supporting Information. Because the interpretation of this transition was already presented in our previous work,[23] we do not further discuss it here. In terms of LMO bases, the PMOV-LMO choice also provides a fairly compact representation of the specific rotation, as only three transitions are sufficient to be within 30% of the converged value (see Figure 1). The isodensity plots for the four LMOs involved in the transitions and the electric and magnetic dipoles are shown in Figure 2. Unless explicitly noted, the electric and magnetic dipoles shown in this and in the following figures are unscaled.

As expected, the transitions involve orbitals localized on the carbonyl and alkene groups. All $\tilde{S}_k$ values have the same sign, as the angle between the vectors is <90°. Transitions (1) and (3) indicate a charge transfer from the carbonyl to the alkene group and vice versa, with a rotation of the orbital density along the carbonyl group; transition (2) is of $\pi \rightarrow \pi^*$ nature, and it would have no contribution to $[\alpha]_D$ in a symmetric alkene group (e.g., ethylene) where the two vectors would be perfectly orthogonal to each other, but it presents a non-negligible $\tilde{S}_k$ value in this case because of the geometrical distortion introduced by the cage structure. The other choices of orbital localization do not offer a similarly compact representation of the tensor, as at least 7−8 transitions need to be considered at once.

We repeat a similar analysis for [8]helicene, with the $\tilde{S}_k$ contributions to $[\alpha]_D$ reported in Figure 3. The CMO basis

DOI: 10.1021/acs.jpca.9b01823
J. Phys. Chem. A 2019, 123, 4406−4418

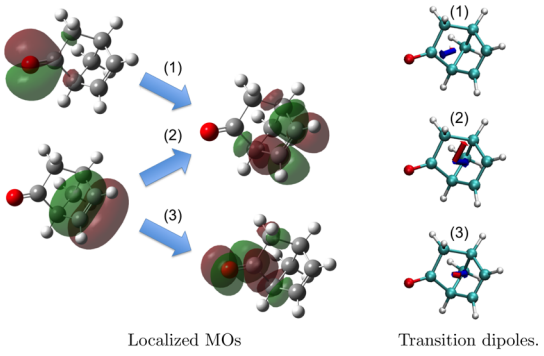

Figure 2. Transitions with the largest $\tilde{S}_k$ values for (1*S*,4*S*)-norbornenone using PMOV-LMOs. Left: Occupied and virtual LMOs; right: electric (red) and magnetic (blue) transition dipole moments.

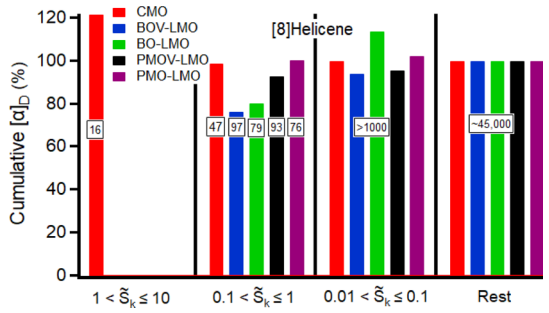

Figure 3. Plot of the cumulative % $\tilde{S}_k$ contributions to the total $[\alpha]_D$ for [8]helicene with various choices of MO basis. The $\tilde{S}_k$ contributions are divided according to their magnitude as reported in the *x* axis labels, whereas the y axis reports the cumulative percent of $[\alpha]_D$ recovered by summing all $\tilde{S}_k$ in the current and larger-value ranges. The numbers on the bars indicate how many transitions fall within each range.

provides the most compact representation of the specific rotation, with 16 transitions necessary to get within 20% of the converged $[\alpha]_D$ value. As described more in detail in the next section, these orbitals are delocalized over a large part of the molecule and not all of the 16 $\tilde{S}_k$ values need to be discussed individually as they correspond to transitions similar in nature. On the other hand, none of the LMO bases provides a compact decomposition of the specific rotation, as at least 76 $\tilde{S}_k$ values are necessary to reproduce $[\alpha]_D$ (with PMO-LMO). Such large number would make the analysis rather cumbersome even if the individual MOs are localized. This result is not completely surprising, as delocalized CMOs can describe rather complex orbital density motion across the molecular frame all at once. This complex motion is fragmented into many contributions using a LMO picture, resulting in many $\tilde{S}_k$ values of comparable magnitude that need to be analyzed explicitly. This trend holds for all of the other helicene compounds considered in this study, as shown in Figures S2−S6 in the Supporting Information; thus, we will continue the discussion only in terms of the CMO results. Additional plots detailing the $\tilde{S}_k$ contributions to $[\alpha]_D$ in the CMO basis (divided by $\tilde{S}_k$ magnitude) for all compounds are reported in Figures S7−S9 of the Supporting Information.

4.2. Helicenes. Helicenes possess strong optical activity, leading to large $[\alpha]_D$, which is clearly due to the intrinsically chiral helical structure of these compounds. However, it is interesting to understand whether this strong chiral response is primarily due to the electric or magnetic dipole components or their relative orientation. At the same time, it is important to determine how the optical response changes with functionalization of these molecules, as this can provide useful insight for the design of compounds with targeted electronic characteristics. Thus, we consider unfunctionalized helicenes (in Section 4.2.1) as well as their functionalized equivalent with both electron-withdrawing: benzothiadiazole (BTD), and electron-donating groups: two thiol groups (in Sections 4.2.2 and 4.2.3). For the functionalized species, we consider both mono- and bis-substitution. We compare molecules of similar molecular mass because $[\alpha]_D$ is inversely proportional to this quantity (see Table S1). Thus, we consider the dithiol group as equivalent to a phenyl ring unit, and a BTD group as equivalent to two phenyl ring units. In other words, we compare the results for [*N*]helicene (where *N* is the number of phenyl units) with those for dithiol[$N-1$]helicene, BTD[$N-2$]helicene, bis-dithiol[$N-2$]helicene, bis-BTD[$N-4$]-helicene, and dithiol-BTD[$N-3$]helicene. The structure of the compounds for $N = 6$ is shown in Figure 4, and the calculated $[\alpha]_D$ values for all helicenes are shown in Figure 5.

Using the $\tilde{S}_k$ analysis, we can separate the contributions to $[\alpha]_D$ in two categories: one where the magnetic vector is aligned with the helical main axis, Type A, and one where it is

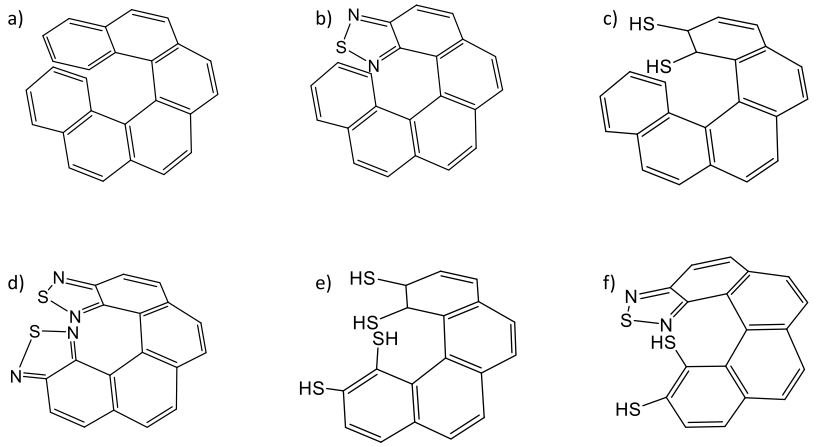

Figure 4. Structures of the $N = 6$ forms of the various helicenes discussed in this work. (a) [6]helicene, (b) BTD[4]helicene, (c) dithiol[5]helicene, (d) bis-BTD[2]helicene, (e) bis-dithiol[4]helicene, and (f) dithiol-BTD[3]helicene.

DOI: 10.1021/acs.jpca.9b01823
J. Phys. Chem. A 2019, 123, 4406−4418

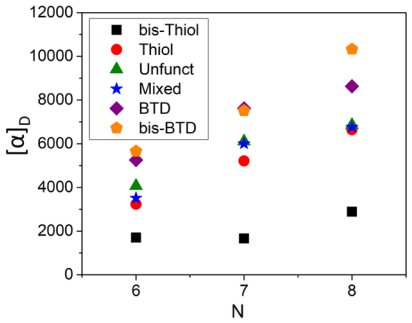

Figure 5. Calculated $[\alpha]_D$ (deg [dm (g/mL)]$^{-1}$) for the helicenes in this study. Unfunct: [N]helicene; Thiol: dithiol[$N-1$]helicene; BTD: BTD[$N-2$]helicene; Bis-Thiol: bis-dithiol[$N-2$]helicene; Bis-BTD: bis-BTD[$N-4$]helicene; and Mixed: dithiol-BTD[$N-3$]helicene.

not, Type B; the latter can be further separated in two subcategories: one where the magnetic vector is orthogonal to the helical main axis, Type B_s, and one where the magnetic vector is tilted with respect to the helical main axis (usually by an angle $0° < \phi < 90°$), Type B_a. The s subscript stands for *symmetric* because these transitions are significant in molecules with the same terminal groups (and the magnetic vector coincides with the C_2 rotational axis), whereas the a subscript stands for *asymmetric* because these transitions are significant for compounds with different terminal groups. The transition types are shown schematically in Figure 6.

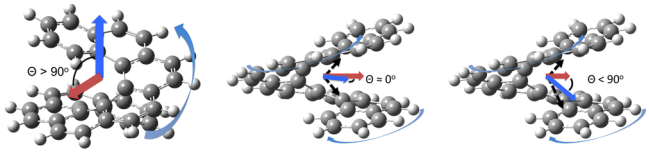

(a) Type A (b) Type B_s (c) Type B_a

Figure 6. Types of transitions that dominate the contribution to $[\alpha]_D$ (a) Type A, (b) Type B_s, and (c) Type B_a. Curved arrows represent the motion of the orbital density associated with the transition, whereas straight arrows represent the total magnetic (blue) and electric (red) dipoles. The black dashed arrows represent local magnetic moments for half-rotations of the orbital density.

Type A transitions are characterized by orbital density moving up or down the body of the helix and involve MOs generally delocalized over several fused rings, which explains the parallel orientation of the magnetic dipole with the helical axis. At the same time, the MO centroids also move along the helix, so that the transition electric dipole moment is tilted with respect to the helical axis. The angle θ between the two dipoles is consistently >90°, corresponding to a negative $\tilde{S}_k$ value that increases the $[\alpha]_D$ magnitude (the two quantities are related through a minus sign, see eq 7). In this type of transition, the direction of the orbital density motion (up or down the helix body) is not important, as the angle between the electric and magnetic vectors is always obtuse, and the $\tilde{S}_k$ sign is consistently negative. Type B transitions can be interpreted as the combination of two separate rotations of the orbital density along the two-halves of the helix. Each half-rotation may be qualitatively described by a local magnetic vector that is tilted with respect to the main helical axis. In B_s transitions, where the terminal groups of the helicene are the same, the tilting angle has the same magnitude for both local magnetic vectors (i.e., ϕ and $\pi-\phi$), so that the components of these vectors parallel to the helical axis cancel out, and the resulting magnetic vector is perpendicular to the helical axis (see Figure 6b). In B_a transitions, where the terminal groups are different, the tilting angles of the local magnetic vectors are different in magnitude so that the cancellation of the components parallel to the helical axis is not perfect, and the resulting magnetic vector is also tilted (see Figure 6c). In either case, the electric vectors tend to be orthogonal to the main helical axis or have orientations similar to that in the Type A transitions. The result is that the overall angle θ between the electric and magnetic dipoles is always acute; thus, the corresponding $\tilde{S}_k$ contributions decrease the $[\alpha]_D$ magnitude. However, given that the magnetic vectors are typically smaller in magnitude compared to those in the Type A transitions (due to the partial or complete cancellation of the components parallel to the helical axis in the vector sum of the local magnetic dipoles), the $\tilde{S}_k$ values for the Type B transitions are also smaller in magnitude than those for the Type A transitions. Hence, Type A transitions dominate the contribution to $[\alpha]_D$, and they determine its sign.

In the following sections, we compare the $[\alpha]_D$ values with the most important $\tilde{S}_k$ contributions in a single plot for each class of helicenes. Because $[\alpha]_D$ is an intensive property, whereas the $\tilde{S}_k$ values are extensive quantities and they are opposite in sign, see eq 7, the plots report $-\tilde{S}_k/M$ rather than just $\tilde{S}_k$. Although $[\alpha]_D$ and $\tilde{S}_k$ have different units, the reported values are proportional through the C_ω factor in eq 7; in other words, the sum of all $-\tilde{S}_k/M$ terms would provide values coincident with the $[\alpha]_D$ values in the plots. The same figures also include the decomposition of each $\tilde{S}_k$ value in terms of the magnitude of the electric and magnetic dipoles as well as the cosine of the angle θ between the two vectors. The scope of these plots is to identify the main $\tilde{S}_k$ terms according to the transition type and to understand which element of the dot product between the transition dipoles is responsible for the trend of $\tilde{S}_k$ (and ultimately $[\alpha]_D$) with N. The magnitude of the electric and magnetic dipoles as well as of $-\cos\theta$ is scaled by $M^{1/3}$ so that their product equals the corresponding $-\tilde{S}_k/M$ value. The numerical values associated with these plots are reported in Tables S2–S8 of the Supporting Information. Because all relevant transitions fall into one of the three categories discussed above (Type A, B_s, or B_a), we focus on the transitions with the largest $\tilde{S}_k$ value for the detailed discussion of the calculations on each set of molecules. For the figures that depict MO isodensity plots, we focus on a representative member of the set because the MOs look similar across helicene lengths.

4.2.1. Unfunctionalized Helicenes. [N]Helicenes are the most basic helicenes. The calculated $[\alpha]_D$ at this level of theory is in good agreement with the experiment, as shown in Figure S10 in the Supporting Information.[42,59,60] Figure 7 reports plots of $[\alpha]_D$ for all unfunctionalized helicenes, including the main $\tilde{S}_k$ contributions and their sum, when more than one transition is important. A good qualitative agreement with the $[\alpha]_D$ trend is obtained with four transitions for [6]helicene (three Type A and one Type B_s), two transitions for [7]helicene (one Type A and one Type B_s), and five transitions for [8]helicene (three Type A and two Type B_s). An example of Type A and Type B_s transitions is reported in Figures S11 and S12 of the Supporting Information, which show the orbital isodensity and vector orientations.

DOI: 10.1021/acs.jpca.9b01823
J. Phys. Chem. A 2019, 123, 4406–4418

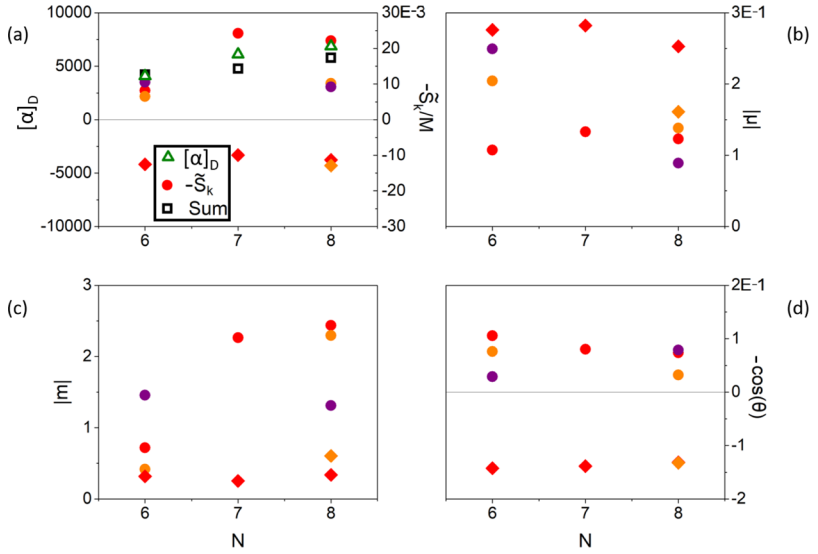

Figure 7. Detailed decomposition of $[\alpha]_D$ for [N]helicenes. (a) $[\alpha]_D$ (deg [dm (g/mL)]$^{-1}$): green triangles; individual $-\tilde{S}_k/M$ values: circles (Type A) and diamonds (Type B_s), where colors distinguish transitions of the same type across subfigures; sum of $-\tilde{S}_k/M$ values: black squares. The other panels represent the electric dipole magnitude (b), magnetic dipole magnitude (c), and $-\cos\theta$ (d), where θ is the angle between the dipole vectors, for each transition, all scaled by $M^{1/3}$. The transitions presented in (a) recover 103.5, 78.0, and 84.3% of the total $[\alpha]_D$ for N = 6−8, respectively.

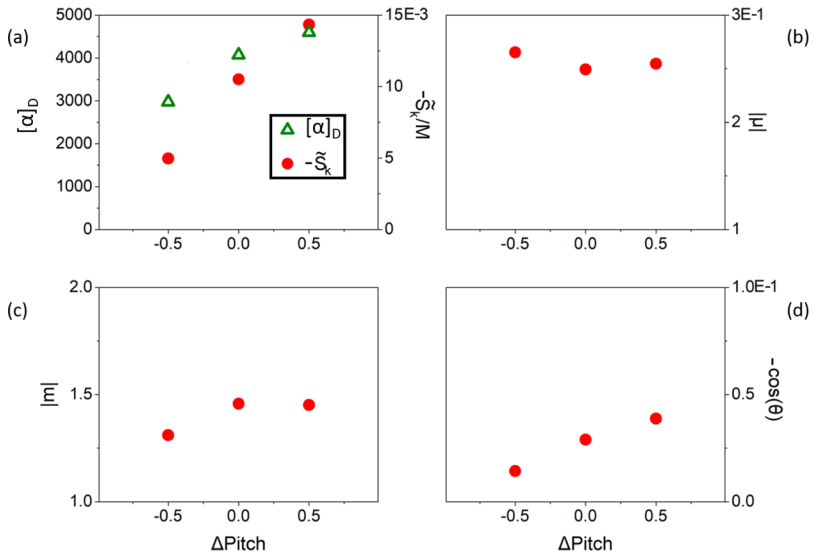

Figure 8. Detailed decomposition of $[\alpha]_D$ for [6]helicene with different pitches. (a) $[\alpha]_D$ (deg [dm (g/mL)]$^{-1}$): green triangles; individual $-\tilde{S}_k/M$ values: circles (Type A). The other panels represent the electric dipole magnitude (b), magnetic dipole magnitude (c), and $-\cos\theta$ (d), where θ is the angle between the dipole vectors, for each transition, all scaled by $M^{1/3}$. The three transitions presented in (a) recover 55.6, 85.9, and 103.9% of the total $[\alpha]_D$ for Δpitch = −0.5, 0, and +0.5 Å, respectively.

As mentioned above, Type A transitions increase the magnitude of $[\alpha]_D$, whereas Type B_s transitions decrease it. For the larger helicenes (N = 7 and 8), there is one very large Type A transition that dominates, which corresponds to a rotation of the orbital density over the entire body of the helix. The spatial extension of both the occupied and virtual MOs over the entire molecule is favored by the overlap of the terminal phenyl rings (see Figure S13 in the Supporting Information). Such overlap is not possible in the smaller helicene, so that the Type A $\tilde{S}_k$ contributions are all relatively small (2−4 a.u.); nevertheless, there is a considerable number of such transitions so that their collective contribution to $[\alpha]_D$ overcomes that of the large Type B_s $\tilde{S}_k$s. When we analyze the magnitude of the $\tilde{S}_k$ values in terms of the components of the vector dot product, we notice that the Type B_s transitions have similar values across the helicene set because the magnitude of the dipole vectors and the angle θ are not significantly influenced by the helical length. This is reasonable because increasing the number of phenyl ring units increases the molecular length only along the main helical axis, but the vectors involved in the Type B_s transitions do not have any component along that direction (see Figure 6). On the other hand, the magnitude of Type A $\tilde{S}_k$ values is strongly correlated with the magnitude of the magnetic dipole, which increases considerably with the helicene length. At the same time, the electric dipole and the angle θ are not strongly influenced by the helical length because the latter does not affect the distance between the orbital centroids (at least for the range of N value considered in this work). Note that the electric dipoles for various transitions point in different directions depending on

DOI: 10.1021/acs.jpca.9b01823
J. Phys. Chem. A 2019, 123, 4406−4418

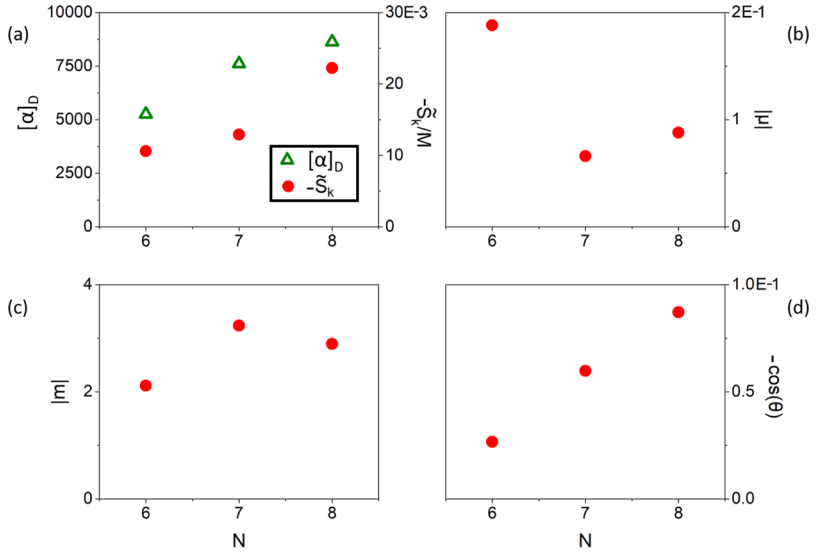

Figure 9. Detailed decomposition of $[\alpha]_D$ for BTD[N − 2]helicenes. (a) $[\alpha]_D$ (deg [dm (g/mL)]$^{-1}$): green triangles; individual $-\tilde{S}_k/M$ values: circles (Type A), where colors distinguish transitions of the same type across subfigures; sum of $\tilde{S}_k$ values: black squares. The other panels represent the electric dipole magnitude (b), magnetic dipole magnitude (c), and $-\cos\theta$ (d), where θ is the angle between the dipole vectors, for each transition, all scaled by $M^{1/3}$. The three transitions presented in (a) recover 67.1, 56.5, and 85.8% of the total $[\alpha]_D$ for N = 6−8, respectively.

the relative position of the MO centroids, but the angle from the helical axis (and thus the angle θ with the corresponding magnetic vector) is rather constant.

It is well known that a parameter that determines the magnitude of $[\alpha]_D$ in helicenes is the helical pitch: the larger the pitch, the larger the $[\alpha]_D$ magnitude. We investigate this trend using [6]helicene, where we perform a constrained geometry optimization by fixing the distance between two C centers one full-turn apart at the equilibrium distance, and at ±0.5 Å from equilibrium. The $\tilde{S}_k$ analysis shows that one leading Type A transition changes significantly (although the orbitals involved remain qualitatively of the same nature and shape), becoming more and more dominant with increasing pitch (see Figure 8). The $\tilde{S}_k$ decomposition clearly shows that its magnitude is mostly influenced by the angle θ between the electric and magnetic vectors, whose relative changes in magnitude largely compensate each other. More specifically, it is the direction of the electric dipole that determines the change in angle because of the change in position of the MO centroids, whereas the direction of the magnetic dipole remains parallel to the helical axis. Thus, the change of $[\alpha]_D$ with the helical pitch is a geometric rather than an electronic effect.

4.2.2. Monofunctionalized Helicenes. In this section and the next, we investigate the factors that determine the changes in $[\alpha]_D$ because of functionalization. As mentioned in Section 4.2, we use BTD as a π-electron-withdrawing group and two thiol units as π-electron-donating groups.

The BTD group increases $[\alpha]_D$ compared to the unfunctionalized helicene analogues, as shown in Figure 5. A more detailed representation of the results for the BTD[N − 2]helicenes is reported in Figure 9. This figure indicates that Type A transitions dominate the $\tilde{S}_k$ contributions to $[\alpha]_D$, and only one transition is necessary to reproduce the qualitative trend with N. The magnitude of the electric and magnetic dipoles is similar to that of [N]helicenes, with the former decreasing and the latter increasing with increasing N. At the same time, the angle between the vectors increases with N. This behavior can be explained by considering the orbitals involved in Type A transitions explicitly, and an example for BTD[6]helicene is shown in Figure 10. The presence of the

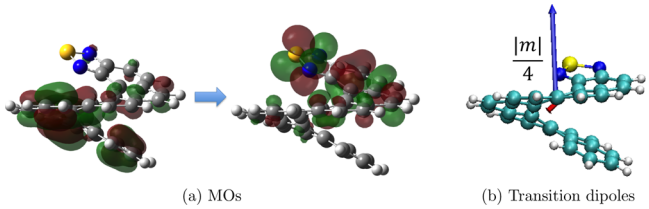

Figure 10. MOs (a), and electric (red) and magnetic (blue) transition dipole vectors (b) for a Type A transition of BTD[6]helicene.

electron-withdrawing group tends to localize the virtual MO on the BTD unit, whereas the occupied MO is still delocalized across the helix, albeit to a lesser degree than in the unfunctionalized helicene analogue. Overall, the $\tilde{S}_k$ value for this transition is similar to that of [6]helicene. However, with increasing N, the more localized nature of the virtual MO simultaneously induces: (1) a longer rotation around the helix body compared to the corresponding [N]helicenes, thus slightly longer magnetic vectors by a factor of 1.2−1.45; (2) shorter electric dipole vectors because the orbital centroids get closer to each other; and (3) larger angles θ, as the electric dipoles become more aligned with the helical axis while pointing away from the magnetic vector. At the same time, the asymmetry in the terminal groups of BTD[N − 2]helicenes changes the Type B_s transitions into B_a transitions. The latter have $\tilde{S}_k$ values that are opposite in sign compared to the Type A transitions and smaller in magnitude compared to both Type A and B_s transitions because the angle between the vectors is closer to 90° (see Figure 6). Taken together, strong Type A and weak Type B_a contributions result in an overall increase in the $[\alpha]_D$ magnitude of BTD[N − 2]helicene compared to [N]helicenes by a factor of 1.25−1.3.

Figure 5 shows that $[\alpha]_D$ for dithiol[N − 1]helicenes is reduced by 5−20% compared to that of the [N]helicenes. Figure 11 indicates that a single Type A transition recovers a

DOI: 10.1021/acs.jpca.9b01823
J. Phys. Chem. A 2019, 123, 4406−4418

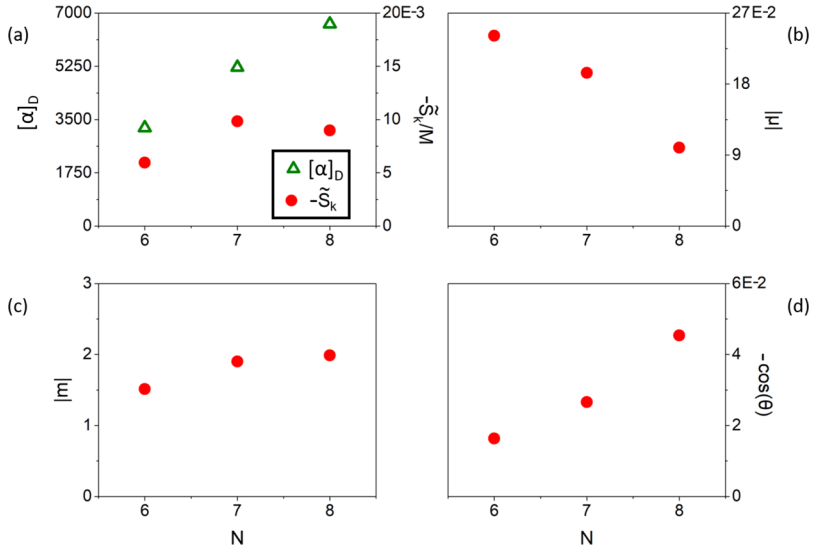

Figure 11. Detailed decomposition of $[\alpha]_D$ for dithiol[7]helicene. (a) $[\alpha]_D$ (deg [dm (g/mL)]$^{-1}$): green triangles; individual $-\tilde{S}_k/M$ values: red circles (Type A). The other panels represent the electric dipole magnitude (b), magnetic dipole magnitude (c), and $-\cos\theta$ (d), where θ is the angle between the dipole vectors, for each transition, all scaled by $M^{1/3}$. The three transitions presented in (a) recover 61.4, 62.8, and 45.0% of the total $[\alpha]_D$ for N = 6−8, respectively.

significant portion of the $[\alpha]_D$ for each of the three helicenes, although reproducing the internal trend passing from N = 7−8 requires more than one transition. This is because the Type A $\tilde{S}_k$ values are overall smaller for the dithiol set than for the others; thus, their relative importance compared to smaller $\tilde{S}_k$ contributions is decreased. Nevertheless, the examination of a single Type A transition is sufficient to explain the overall smaller values of $[\alpha]_D$ for the dithiol set compared to the unfunctionalized helicenes. The trends for the vector magnitudes and relative angles, also in Figure 11, are similar to those for BTD[N − 2]helicenes (see Figure 9). The main difference is that the magnitude of the magnetic dipoles and the angle θ are smaller with the dithiol groups than with BTD. The reason for this change can be understood by considering the orbitals involved in a typical transition, shown in Figure 12.

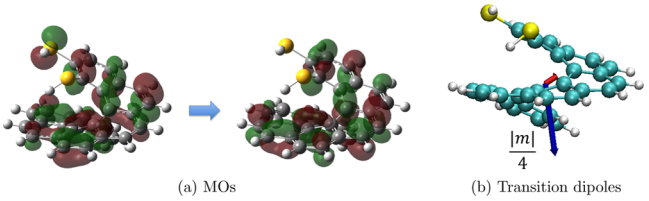

Figure 12. MOs (a), and electric (red) and magnetic (blue) transition dipole vectors (b) for a Type A transition of dithiol[7]helicene.

With dithiol, it is the occupied MO that is now more localized on the substituent group. However, because dithiol is a weaker electron-donating group than BTD is an electron-withdrawing group (compare the atomic charges of the bridging carbons of BTD, phenyl, and dithiol model systems in Figure S14 of the Supporting Information),[61,62] the localization is not as strong as in the BTD[N − 2]helicenes. This leads to the smaller magnetic dipole and angle θ values, and ultimately $\tilde{S}_k$ and $[\alpha]_D$ values, even if the trends are consistent for both choices of substituents. Furthermore, as for BTD, Type B_a transitions also tend to decrease $[\alpha]_D$ and their relative importance is larger because the Type A $\tilde{S}_k$ values are smaller. Compared to [N]helicenes, the relative smaller magnitude of the magnetic dipoles of the dithiol[N − 1]helicenes and the compensating changes in the electric dipole magnitude and angle θ lead to overall smaller $[\alpha]_D$ values. However, the weak electron-donating nature of the dithiol group also leads to a smaller deviation from the [N]helicenes $[\alpha]_D$ values compared to BTD[N − 2]helicenes.

4.2.3. Bis-Functionalized Helicenes. We now consider the functionalized helicenes with two substituent groups at both ends of the helix: bis-BTD[N − 4]helicenes, bis-dithiol[N − 2]helicenes, and mixed dithiol-BTD[N − 3]helicenes. The corresponding $[\alpha]_D$ values are plotted in Figure 5. The specific rotation for the bis-BTD species with for N = 6 and 7 is similar in magnitude to that of the corresponding mono-BTD species, but it is larger by 20% for the N = 8 compound. The detailed component separation for the $\tilde{S}_k$ values of the bis-BTD[N − 4]helicenes is reported in Figure 13, where it is clear that one Type A transition dominates. Although for these transitions the magnetic dipole moment is parallel to the helical axis, they can also be described as two half-rotations of the orbital density from the central rings toward the terminal BTD groups, where the virtual MOs are localized, see Figure 14 for the N = 8 case. Contrary to regular Type B_s transitions, the overlap of the virtual MO region in between the BTD units can be described as a phase change for one of the half-rotations, which in turn changes the direction of the corresponding local magnetic dipole moment. Therefore, the components of the local magnetic dipoles that are parallel to the helical axis add up, whereas the component orthogonal to that axis cancel out, resulting in a total magnetic dipole parallel to the helical axis as in a typical Type A transition. The overlap of the BTD groups is particularly large for bis-BTD[4]helicenes (i.e., N = 8), which produces a strong pull for the half rotations, and a particularly large magnetic dipole moment and related $\tilde{S}_k$ value. On the other hand, the resulting magnetic dipole for the N = 6 and 7 species is of the same magnitude of that for the mono-BTD species, whereas the changes in electric dipole magnitude and angle θ compensate each other. As a result, $[\alpha]_D$ for the mono and bis-BTD compounds with N = 6 and 7 is similar in magnitude. Note that for bis-BTD[N − 4]helicenes, there are

DOI: 10.1021/acs.jpca.9b01823
J. Phys. Chem. A 2019, 123, 4406−4418

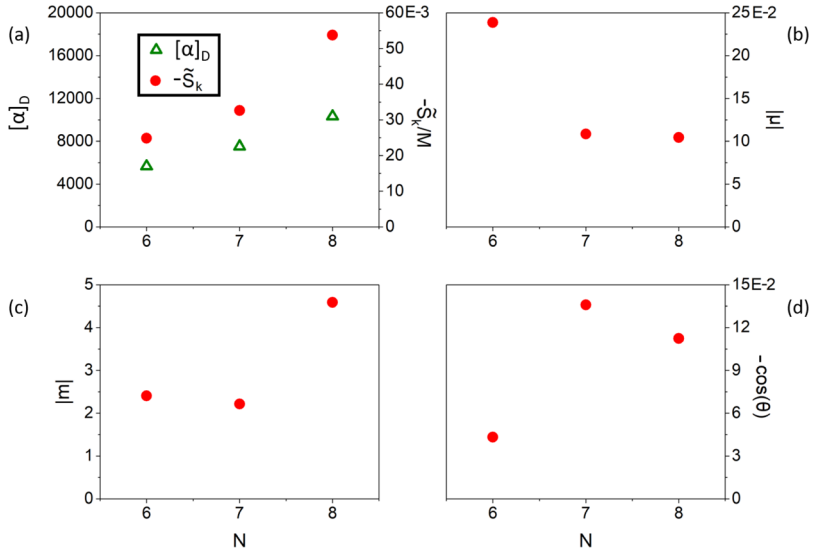

Figure 13. Detailed decomposition of $[\alpha]_D$ for bis-BTD[N − 4]helicenes. (a) $[\alpha]_D$ (deg [dm (g/mL)]$^{-1}$): green triangles; individual $-\tilde{S}_k/M$ values: red circles (Type A). The other panels represent the electric dipole magnitude (b), magnetic dipole magnitude (c), and −cos θ (d), where θ is the angle between the dipole vectors, for each transition, all scaled by $M^{1/3}$. The three transitions presented in (a) recover 146.6, 144.7, and 173.5% of the total $[\alpha]_D$ for N = 6−8, respectively.

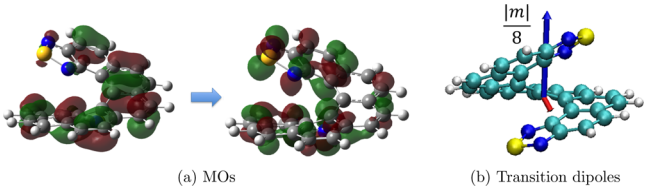

Figure 14. MOs (a), and electric (red) and magnetic (blue) transition dipole vectors (b) for a Type A transition of bis-BTD[4]helicene.

important contributions from Type B_s transitions, given that these compounds belong to the same point group as [N]helicenes, but these contributions are compensated by a number of smaller Type A $\tilde{S}_k$ terms (not shown).

Figure 15 reports the detailed data for the largest $\tilde{S}_k$ contributions for bis-dithiol[N − 2]helicenes. Also in this case, one Type A transition dominates. These compounds are characterized by a $[\alpha]_D$ that is reduced further from the dithiol compounds by 50−70% because of smaller Type A $\tilde{S}_k$ contributions. These Type A transitions are similar in nature to those for the bis-BTD species, as shown in Figure 16 for a typical case, except that now it is the occupied MO that is mostly localized at the edges of the helix (i.e., on the dithiol group), whereas the virtual MO is more localized toward the central rings. However, the same discussion in terms of the sum of two half-rotations applies here as well to describe the contributions to the $\tilde{S}_k$ value. As for the mono-substituted helicenes, the dithiol group is a weaker directing group than

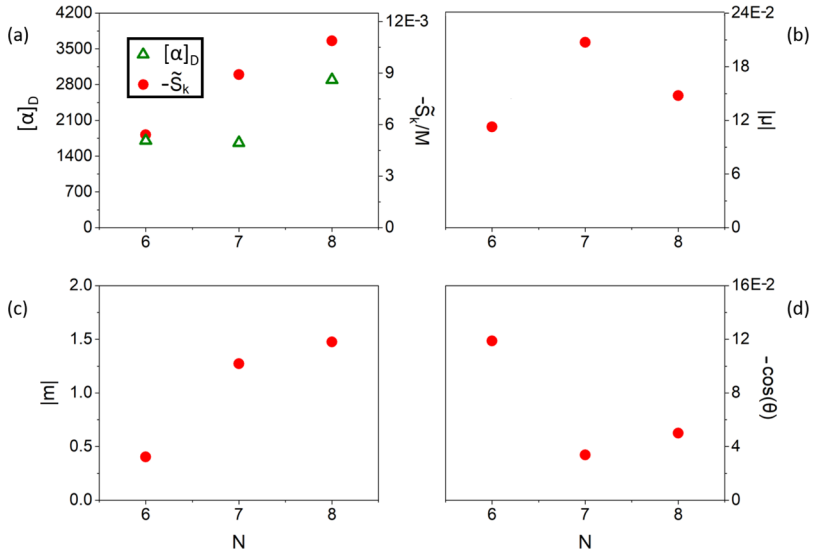

Figure 15. Detailed decomposition of $[\alpha]_D$ for bis-dithiol[N − 2]helicenes. (a) $[\alpha]_D$ (deg [dm (g/mL)]$^{-1}$): green triangles; individual $-\tilde{S}_k/M$ values: red circles (Type A). The other panels represent the electric dipole magnitude (b), magnetic dipole magnitude (c), and −cos θ (d), where θ is the angle between the dipole vectors, for each transition, all scaled by $M^{1/3}$. The three transitions presented in (a) recover 105.9, 178.6, and 125.4% of the total $[\alpha]_D$ for N = 6−8, respectively.

DOI: 10.1021/acs.jpca.9b01823
J. Phys. Chem. A 2019, 123, 4406−4418

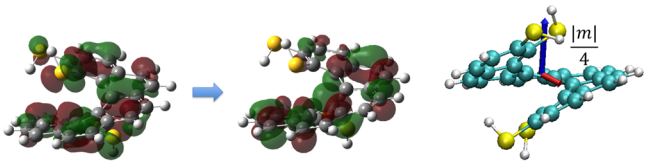

Figure 16. MOs (a), and electric (red) and magnetic (blue) transition dipole vectors (b) for a Type A transition of bis-dithiol[6]helicene.

BTD, so that the resulting magnetic dipole moments are smaller in magnitude. Although we limited the analysis to the largest Type A $\tilde{S}_k$ value, we note that a significant number of Type A and B_s transitions contribute to $[\alpha]_D$ with $\tilde{S}_k$ values that are similar in magnitude and opposite in sign, so that they mostly cancel out.

The $[\alpha]_D$ values for the mixed dithiol-BTD[$N-3$]helicenes are very close to those of [N]helicenes (for $N = 6$, $[\alpha]_D$ is smaller by 13.5%, whereas for $N = 7,8$, $[\alpha]_D$ is smaller by only 1.5%), as reported in Figure 5. The trend of $[\alpha]_D$ with N for the dithiol-BTD compounds is reported in Figure 17 with the usual main contribution from a Type A transition. Similar to other cases, the trend in $\tilde{S}_k$ is determined by the length of the magnetic dipole, which increases with the length of the helix. However, the overall magnitude of the magnetic dipole is in general larger than the equivalent transitions in the unfunctionalized helicenes. The reason why the final $[\alpha]_D$ values are similar between these two sets of compounds is the angle θ, which is closer to 90° in the dithiol-BTD set. This is due to the asymmetry of the substituent groups, which affects the orbital density rotation around the helix body and results in a magnetic dipole that is slightly tilted away from the helical axis. This is an electronic effect rather than a geometrical one. It can be shown by replacing the dithiol groups in the dithiol-BTD[5]helicene with a regular fused phenyl unit and reoptimizing the geometry of the new C and H centers while keeping the rest frozen (in other words, we constructed a BTD[6]helicene with the same pitch as the original dithiol-BTD[5]helicene). The magnetic dipoles in the original and modified structures are close in magnitude, but in the latter, the dipole is less aligned with the helical axis, thus reducing the angle θ with the electric dipole, see Figure S15 in the Supporting Information.

5. DISCUSSION AND CONCLUSIONS

In this work, we present an analysis of $[\alpha]_\omega$ of helicenes in terms of $\tilde{S}_k$ contributions, which allow the decomposition of this property according to one-electron excitations between MOs. We show that such analysis can be performed with different choices of MO representation. For helicenes, CMOs are the best choice because delocalized π orbitals offer the most natural and compact decomposition of the specific rotation. However, LMOs are likely better for molecules with small functional groups, where LMOs may provide a more chemically intuitive partitioning of $[\alpha]_D$.

We focus on [N]helicenes with $N = 6-8$ as well as analogous functionalized species, where electron-withdrawing and donating groups direct the movement of the electron density and therefore affect $[\alpha]_D$. The scope is to determine how the rotation changes with N and with the functionalization groups. We find that the major contributions to $[\alpha]_D$ come from three types of transitions, categorized depending on the orientation of the magnetic dipole term: parallel to the helical axis (Type A), orthogonal to the helical axis (Type B_s), and tilted (Type B_a) (see Figure 6). Type A contributions are the strongest and determine the sign of the rotation. Type B transitions are progressively weaker and have the opposite sign, thus reducing the magnitude of $[\alpha]_D$. In particular, Type B_s transitions are present in symmetric compounds (i.e., those with the same terminal groups and C_2 symmetry), whereas Type B_a transitions occur in asymmetric compounds (i.e., those with different terminal groups).

Type A transitions are mostly characterized by movement of the electron along the entire body of the helix, thus generating a large magnetic response along the helical axis. The magnitude of these transitions increases with N because the electron can

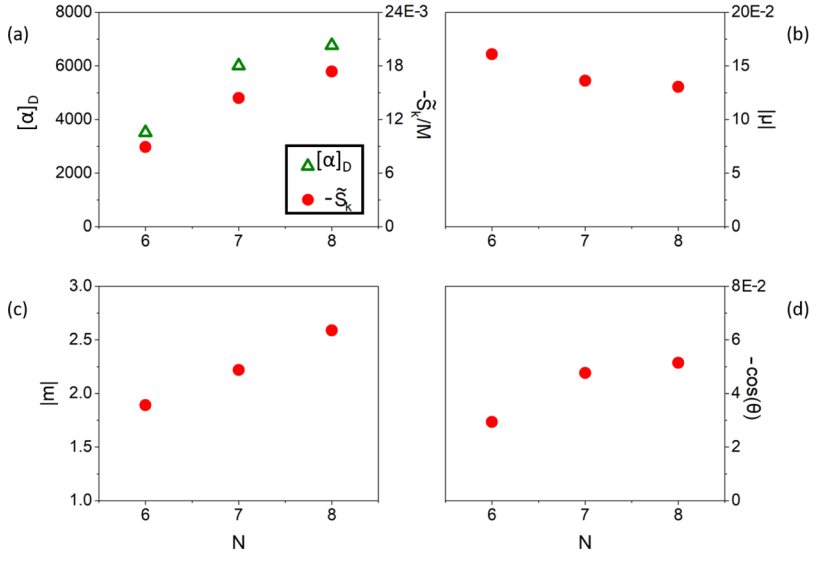

Figure 17. Detailed decomposition of $[\alpha]_D$ for dithiol-BTD[$N-3$]helicenes. (a) $[\alpha]_D$ (deg [dm (g/mL)]$^{-1}$): green triangles; individual $-\tilde{S}_k/M$ values: red circles (Type A). The other panels represent the electric dipole magnitude (b), magnetic dipole magnitude (c), and $-\cos\theta$ (d), where θ is the angle between the dipole vectors, for each transition, all scaled by $M^{1/3}$. The three transitions presented in (a) recover 84.6, 80.0, and 85.6% of the total $[\alpha]_D$ for $N = 6-8$, respectively.

DOI: 10.1021/acs.jpca.9b01823
J. Phys. Chem. A 2019, 123, 4406−4418

move further, and their $\tilde{S}_k$ values are strongly dominated by the magnitude of the magnetic dipole. Terminal substituents affect this type of transition by a tendency to localize the occupied or virtual MOs on the group. For strong groups (BTD), this increases the extent of the motion along the body of the helix compared to the unfunctionalized helicene analogues, thus increasing the magnitude of the magnetic dipole and the corresponding $\tilde{S}_k$ value. In turn, this results in an overall increase of the specific rotation. For weaker groups (dithiol), the partial localization reduces the extent of the motion along the body of the helix, thus resulting in smaller $[\alpha]_D$. Bis-functionalization induces Type A transitions with large $\tilde{S}_k$ values that may be described by simultaneous half-rotations of the electron from the terminal groups to the central rings, and vice-versa. In these half-rotations, the local magnetic dipoles sum constructively (thanks to a phase change in one of the MOs). The resulting $\tilde{S}_k$ values may be smaller, similar, or larger than those of the corresponding unfunctionalized helicenes depending on the strength of the terminal groups and the degree of overlap between these groups. Specifically, bis-dithiol substitution leads to smaller $[\alpha]_D$ than the [*N*]helicenes analogues (see Figure 15); bis-BTD substitution leads to similar values of $[\alpha]_D$ for $N = 6$, 7 and larger values of $[\alpha]_D$ for $N = 8$ (due to the overlap between the terminal BTD moieties) (see Figure 13). Interestingly, a mixed substitution leads to $[\alpha]_D$ values similar to the [*N*]helicenes analogues, see Figure 17, because the magnetic dipoles of the large $\tilde{S}_k$ terms, although larger than that in the unfunctionalized compounds, are tilted away from the helical axis because of the asymmetry of the terminal groups. The analysis of Type A transitions also allows us to show that the helical pitch effect on $[\alpha]_D$ is geometrical rather than electronic, as the magnitude of the electric and magnetic dipole vectors is mostly unchanged, but the angle between the two increases with the pitch (see Figure 8). Type B transitions can be described as two simultaneous half-rotations of the electron along the body of the helix, without phase change of the MOs. This results in complete (B_s) or partial (B_a) cancellation of the magnetic dipole component along the helical axis, which leaves the component perpendicular to the axis dominating. Therefore, these transitions correspond to smaller $\tilde{S}_k$ values than those of Type A. Additionally, the $\tilde{S}_k$ values of Type B transitions are not strongly dependent on N because the length of the helix only affects the contributions that are parallel to the helical axis.

It appears from this analysis that functionalization of the helicenes influences $[\alpha]_D$ in a complex manner, where the strength of the substituent groups and the length of the helix may lead to cooperative or competitive effects. At the same time, the $\tilde{S}_k$ analysis affords a relatively simple interpretation of these effects in terms of one-electron MO transitions. These studies may therefore lead to guidelines for the design of compounds with desired chiroptical responses.

■ ASSOCIATED CONTENT

Supporting Information

The Supporting Information is available free of charge on the ACS Publications website at DOI: 10.1021/acs.jpca.9b01823.

Primary transition in the CMO basis for (1*S*,4*S*)-norbornenone, plots of the cumulative contributions to $[\alpha]_D$ from $\tilde{S}_k$ for the $N = 8$ helicene derivatives with all MO bases, and the same plots for all helicenes with the CMO basis; additionally, it contains a plot comparing experimental and calculated [*N*]helicene $[\alpha]_D$, examples of Type A and Type B_s transitions and MO overlap for [8]helicene, a comparison of the atomic charges of BTD, naphthalene, and dithiol models, and a comparison of the magnetic dipoles for dithiol-BTD[5]helicene and a modified BTD[6]helicene; and finally, it contains tables with the molecular weights of all helicenes, the numerical values of the data reported in Figures 7−9, 11, 13, 15, and 17, as well as the Cartesian coordinates (Å) for the optimized structures (PDF)

■ AUTHOR INFORMATION

Corresponding Author

*E-mail: mcaricato@ku.edu.

ORCID

Marco Caricato: 0000-0001-7830-0562

Notes

The authors declare no competing financial interest.

■ ACKNOWLEDGMENTS

The authors are grateful for support from the National Science Foundation under grant CHE-1650942.

■ REFERENCES

(1) Vaccaro, P. H. In *Comprehensive Chiroptical Spectroscopy, Instrumentation, Methodologies, and Theoretical Simulations*; Woody, B. P. N., Ed.; John Wiley & Sons, 2012; Vol *1*, pp 265−324.

(2) Polavarapu, B. P. L. Ab initio molecular optical rotations and absolute configurations. *Mol. Phys.* **1997**, *91*, 551−554.

(3) Cheeseman, J. R.; Frisch, M. J.; Devlin, F. J.; Stephens, P. J. Hartree-Fock and density functional theory ab initio calculation of optical rotation using GIAOs: basis set dependence. *J. Phys. Chem. A* **2000**, *104*, 1039−1046.

(4) Grimme, S. Calculation of frequency dependent optical rotation using density functional response theory. *Chem. Phys. Lett.* **2001**, *339*, 380−388.

(5) Polavarapu, P. L. Optical rotation: recent advances in determining the absolute configuration. *Chirality* **2002**, *14*, 768−781.

(6) Autschbach, J.; Patchkovskii, S.; Ziegler, T.; van Gisbergen, S. J. a.; Jan Baerends, E. Chiroptical properties from time-dependent density functional theory. II. Optical rotations of small to medium sized organic molecules. *J. Chem. Phys.* **2002**, *117*, 581−592.

(7) Ruud, K.; Helgaker, T. Optical rotation studied by density-functional and coupled-cluster methods. *Chem. Phys. Lett.* **2002**, *352*, 533−539.

(8) Stephens, P. J.; McCann, D. M.; Cheeseman, J. R.; Frisch, M. J. Determination of absolute configurations of chiral molecules using ab initio time-dependent density functional theory calculations of optical rotation: How reliable are absolute configurations obtained for molecules with small rotations? *Chirality* **2005**, *17*, S52−S64.

(9) Grimme, S.; Bahlmann, A.; Haufe, G. n. Ab initio calculations for the optical rotations of conformationally flexible molecules: A case study on six-, seven-, and eight-membered fluorinated cycloalkanol esters. *Chirality* **2002**, *14*, 793−797.

(10) Ruud, K.; Stephens, P. J.; Devlin, F. J.; Taylor, P. R.; Cheeseman, J. R.; Frisch, M. J. Coupled-cluster calculations of optical rotation. *Chem. Phys. Lett.* **2003**, *373*, 606−614.

(11) Tam, M. C.; Russ, N. J.; Crawford, T. D. Coupled cluster calculations of optical rotatory dispersion of (S)-methyloxirane. *J. Chem. Phys.* **2004**, *121*, 3550−3557.

(12) Crawford, T. D. Ab initio calculation of molecular chiroptical properties. *Theor. Chem. Acc.* **2006**, *115*, 227−245.

(13) Crawford, T. D.; Stephens, P. J. Comparison of time-dependent density-functional theory and coupled cluster theory for the

DOI: 10.1021/acs.jpca.9b01823
J. Phys. Chem. A 2019, 123, 4406−4418

calculation of the optical rotations of chiral molecules. *J. Phys. Chem. A* **2008**, *112*, 1339−1345.
(14) Pedersen, T. B.; Koch, H.; Boman, L.; Sánchez de Merás, A. M. J. Origin invariant calculation of optical rotation without recourse to London orbitals. *Chem. Phys. Lett.* **2004**, *393*, 319−326.
(15) Crawford, T. D.; Owens, L. S.; Tam, M. C.; Schreiner, P. R.; Koch, H. Ab initio calculation of optical rotation in (P)-(+)-[4]-triangulane. *J. Am. Chem. Soc.* **2005**, *127*, 1368−1369.
(16) Krykunov, M.; Autschbach, J. Calculation of optical rotation with time-periodic magnetic-field-dependent basis functions in approximate time-dependent density-functional theory. *J. Chem. Phys.* **2005**, *123*, 114103.
(17) Autschbach, J. Computing chiroptical properties with first-principles theoretical methods: background and illustrative examples. *Chirality* **2009**, *21*, E116−E152.
(18) Moore, B.; Srebro, M.; Autschbach, J. Analysis of optical activity in terms of bonds and lone-pairs: The exceptionally large optical rotation of norbornenone. *J. Chem. Theory Comput.* **2012**, *8*, 4336−4346.
(19) Murphy, V. L.; Kahr, B. Hückel theory and optical activity. *J. Am. Chem. Soc.* **2015**, *137*, 5177−5183.
(20) Murphy, V. L.; Farfan, C.; Kahr, B. Chiroptical structure - property relations in cyclo[18]carbon and its in silico hydrogenation products. *Chirality* **2018**, *30*, 325−331.
(21) Wiberg, K. B. Chirality induced by the interaction of C=C and C=X bonds (X=CH2, NH, NH2+, O, and S) separated by a methylene group. *J. Phys. Chem. A* **2016**, *120*, 7771−7777.
(22) Wiberg, K. B. Chiroptical properties of imines derived from R-(+)-norbornenone: The role of electronegativity differences. *J. Phys. Chem. A* **2017**, *121*, 8247−8250.
(23) Caricato, M. Orbital analysis of molecular optical activity based on configuration rotatory strength. *J. Chem. Theory Comput.* **2015**, *11*, 1349−1353.
(24) Caricato, M. Conformational effects on specific rotation: A theoretical study based on the $\tilde{S}_k$ method. *J. Phys. Chem. A* **2015**, *119*, 8303−8310.
(25) Gingras, M. One hundred years of helicene chemistry. Part 1: Non-stereoselective syntheses of carbohelicenes. *Chem. Soc. Rev.* **2013**, *42*, 968−1006.
(26) Furche, F.; Ahlrichs, R.; Wachsmann, C.; Weber, E.; Sobanski, A.; Vögtle, F.; Grimme, S. Circular dichroism of helicenes investigated by time-dependent density functional theory. *J. Am. Chem. Soc.* **2000**, *122*, 1717−1724.
(27) Verbiest, T.; Verbiest, T.; Elshocht, S. V.; Kauranen, M.; Hellemans, L.; Snauwaert, J.; Nuckolls, C.; Katz, T. J. Strong enhancement of nonlinear optical properties through supramolecular chirality. *Science* **1998**, *282*, 913−915.
(28) Bossi, A.; Licandro, E.; Maiorana, S.; Rigamonti, C.; Righetto, S.; Stephenson, G. R.; Spassova, M.; Botek, E.; Champagne, B. Theoretical and experimental investigation of electric field induced second harmonic generation in tetrathia[7]helicenes. *J. Phys. Chem. C* **2008**, *112*, 7900−7907.
(29) Saleh, N.; Vanthuyne, N.; Bonvoisin, J.; Autschbach, J.; Srebro-Hooper, M.; Crassous, J. Redox-triggered chiroptical switching activity of ruthenium(III)-bis-(β-diketonato) complexes bearing a bipyridine-helicene ligand. *Chirality* **2018**, *30*, 592−601.
(30) Bouvier, R.; Durand, R.; Favereau, L.; Srebro-Hooper, M.; Dorcet, V.; Roisnel, T.; Vanthuyne, N.; Vesga, Y.; Donnelly, J.; Hernandez, F.; et al. Helicenes grafted with 1,1,4,4-tetracyanobutadiene moieties: π-helical push-pull systems with strong electronic circular dichroism and two-photon absorption. *Chem.—Eur. J.* **2018**, *24*, 14484−14494.
(31) Biet, T.; Martin, K.; Hankache, J.; Hellou, N.; Hauser, A.; Bürgi, T.; Vanthuyne, N.; Aharon, T.; Caricato, M.; Crassous, J.; et al. Triggering emission with the helical turn in thiadiazole-helicenes. *Chem.—Eur. J.* **2017**, *23*, 437−446.
(32) Dhbaibi, K.; Favereau, L.; Srebro-Hooper, M.; Jean, M.; Vanthuyne, N.; Zinna, F.; Jamoussi, B.; Di Bari, L.; Autschbach, J.; Crassous, J. Exciton coupling in diketopyrrolopyrrole-helicene derivatives leads to red and near-infrared circularly polarized luminescence. *Chem. Sci.* **2018**, *9*, 735−742.
(33) Shen, C.; He, X.; Toupet, L.; Norel, L.; Rigaut, S.; Crassous, J. Dual redox and optical control of chiroptical activity in photochromic dithienylethenes decorated with hexahelicene and bis-ethynyl-ruthenium units. *Organometallics* **2018**, *37*, 697−705.
(34) Hellou, N.; Macé, A.; Martin, C.; Dorcet, V.; Roisnel, T.; Jean, M.; Vanthuyne, N.; Berrée, F.; Carboni, B.; Crassous, J. Synthesis of carbo[6]helicene derivatives grafted with amino or aminoester substituents from enantiopure [6]helicenyl boronates. *J. Org. Chem.* **2018**, *83*, 484−490.
(35) OuYang, J.; Crassous, J. Chiral multifunctional molecules based on organometallic helicenes: Recent advances. *Coord. Chem. Rev.* **2018**, *376*, 533−547.
(36) Hellou, N.; Jahier-Diallo, C.; Baslé, O.; Srebro-Hooper, M.; Toupet, L.; Roisnel, T.; Caytan, E.; Roussel, C.; Vanthuyne, N.; Autschbach, J.; et al. Electronic and chiroptical properties of chiral cycloiridiated complexes bearing helicenic NHC ligands. *Chem. Commun.* **2016**, *52*, 9243−9246.
(37) Shen, C.; Loas, G. h.; Srebro-Hooper, M.; Vanthuyne, N.; Toupet, L.; Cador, O.; Paul, F.; López Navarrete, J. T.; Ramírez, F. J.; Nieto-Ortega, B.; et al. Iron alkynyl helicenes: Redox-triggered chiroptical tuning in the IR and near-IR spectral regions and suitable for telecommunications applications. *Angew. Chem., Int. Ed.* **2016**, *55*, 8062−8066.
(38) Isla, H.; Srebro-Hooper, M.; Jean, M.; Vanthuyne, N.; Roisnel, T.; Lunkley, J. L.; Muller, G.; Williams, J. A. G.; Autschbach, J.; Crassous, J. Conformational changes and chiroptical switching of enantiopure bis-helicenic terpyridine upon Zn2+ binding. *Chem. Commun.* **2016**, *52*, 5932−5935.
(39) Bensalah-Ledoux, A.; Pitrat, D.; Reynaldo, T.; Srebro-Hooper, M.; Moore, B.; Autschbach, J.; Crassous, J.; Guy, S.; Guy, L. Large-scale synthesis of helicene-like molecules for the design of enantiopure thin films with strong chiroptical activity. *Chem.—Eur. J.* **2016**, *22*, 3333−3346.
(40) Shen, C.; Anger, E.; Srebro, M.; Vanthuyne, N.; Toupet, L.; Roussel, C.; Autschbach, J.; Réau, R.; Crassous, J. Diastereo- and enantioselective synthesis of organometallic bis(helicene)s by a combination of C-H activation and dynamic isomerization. *Chem.—Eur. J.* **2013**, *19*, 16722−16728.
(41) Nakai, Y.; Mori, T.; Inoue, Y. Circular dichroism of (di)methyl- and diaza[6]helicenes. A combined theoretical and experimental study. *J. Phys. Chem. A* **2013**, *117*, 83−93.
(42) Nakai, Y.; Mori, T.; Inoue, Y. Theoretical and experimental studies on circular dichroism of carbo[N]helicenes. *J. Phys. Chem. A* **2012**, *116*, 7372−7385.
(43) Tanaka, H.; Kato, Y.; Fujiki, M.; Inoue, Y.; Mori, T. Combined experimental and theoretical study on circular dichroism and circularly polarized luminescence of configurationally robust D3-symmetric triple pentahelicene. *J. Phys. Chem. A* **2018**, *122*, 7378−7384.
(44) Foster, J. M.; Boys, S. F. Canonical configuration interaction procedure. *Rev. Mod. Phys.* **1960**, *32*, 300−302.
(45) Boys, S. F. Construction of some molecular orbitals to be approximately invariant for changes from one molecule to another. *Rev. Mod. Phys.* **1960**, *32*, 296−299.
(46) Pipek, J.; Mezey, P. G. A fast intrinsic localization procedure applicable for ab initio and semiempirical linear combination of atomic orbital wave functions. *J. Chem. Phys.* **1989**, *90*, 4916−4926.
(47) Rosenfeld, L. Quantenmechanische Theorie der natürlichen optischen Aktivität von Flüssigkeiten und Gasen. *Z. Phys.* **1929**, *52*, 161−174.
(48) Wiberg, K. B.; Wang, Y.-g.; Wilson, S. M.; Vaccaro, P. H.; Cheeseman, J. R. Sum-over-states calculation of the specific rotations of some substituted oxiranes, chloropropionitrile, ethane, and norbornenone. *J. Phys. Chem. A* **2006**, *110*, 13995−14002.
(49) Frisch, M. J.; Trucks, G. W.; Schlegel, H. B.; Scuseria, G. E.; Robb, M. A.; Cheeseman, J. R.; Scalmani, G.; Barone, V.; Petersson,

DOI: 10.1021/acs.jpca.9b01823
J. Phys. Chem. A 2019, 123, 4406−4418

G. A.; Nakatsuji, H. et al. *Gaussian Development Version*, Rev. I09, 2016.
(50) Yanai, T.; Tew, D. P.; Handy, N. C. A new hybrid exchange-correlation functional using the Coulomb-attenuating method (CAM-B3LYP). *Chem. Phys. Lett.* **2004**, *393*, 51−57.
(51) Woon, D. E.; Dunning, T. H. Gaussian basis sets for use in correlated molecular calculations. IV. Calculation of static electrical response properties. *J. Chem. Phys.* **1994**, *100*, 2975−2988.
(52) Becke, A. D. A new mixing of Hartree-Fock and local density-functional theories. *J. Chem. Phys.* **1993**, *98*, 1372−1377.
(53) Becke, A. D. Density-functional thermochemistry. III. The role of exact exchange. *J. Chem. Phys.* **1993**, *98*, 5648−5652.
(54) Lee, C.; Yang, W.; Parr, R. G. Development of the Colle-Salvetti correlation-energy formula into a functional of the electron density. *Phys. Rev. B* **1988**, *37*, 785−789.
(55) London, F. Théorie quantique des courants interatomiques dans les combinaisons aromatiques. *J. Phys. Radium* **1937**, *8*, 397−409.
(56) Ditchfield, R. Self-consistent perturbation theory of diamagnetism. *Mol. Phys.* **1974**, *27*, 789−807.
(57) Wiberg, K. B.; Caricato, M.; Wang, Y.-g.; Vaccaro, P. H. Towards the accurate and efficient calculation of optical rotatory dispersion using augmented minimal basis sets. *Chirality* **2013**, *25*, 606−616.
(58) Caricato, M.; Vaccaro, P. H.; Crawford, T. D.; Wiberg, K. B.; Lahiri, P. Insights on the origin of the unusually large specific rotation of (1S,4S)-Norbornenone. *J. Phys. Chem. A* **2014**, *118*, 4863−4871.
(59) Martin, R. H.; Flammang-Barbieux, M.; Cosyn, J. P.; Gelbcke, M. 1-Synthesis of octa- and nonahelicenes. 2-New syntheses of hexa- and heptahelicenes. 3-Optical rotation and O.R.D. of heptahelicene. *Tetrahedron Lett.* **1968**, *9*, 3507−3510.
(60) Martin, R. H.; Libert, V. J. Helicenes - the use of resolved hexahelicene-2-carboxylic acid as a common precursor for the photochemical synthesis of optically pure octa-helicenes, nona-helicenes, deca-helicenes, undeca-helicenes and trideca-helicenes - thermal racemization of deca-helicenes and undeca helicenes. *J. Chem. Res., Miniprint* **1980**, *4*, 1940−1950.
(61) Besler, B. H.; Merz, K. M.; Kollman, P. A. Atomic charges derived from semiempirical methods. *J. Comput. Chem.* **1990**, *11*, 431−439.
(62) Singh, U. C.; Kollman, P. A. An approach to computing electrostatic charges for molecules. *J. Comput. Chem.* **1984**, *5*, 129−145.

DOI: 10.1021/acs.jpca.9b01823
J. Phys. Chem. A 2019, 123, 4406−4418